The use of multiobjective calibration and regional sensitivity analysis in simulating hyporheic exchange

Ramon C. Naranjo,[1,2] Richard G. Niswonger,[2] Mark Stone,[3] Clinton Davis,[4] and Alan Mckay[1]

Received 20 July 2011; revised 20 November 2011; accepted 6 December 2011; published 26 January 2012.

[1] We describe an approach for calibrating a two-dimensional (2-D) flow model of hyporheic exchange using observations of temperature and pressure to estimate hydraulic and thermal properties. A longitudinal 2-D heat and flow model was constructed for a riffle-pool sequence to simulate flow paths and flux rates for variable discharge conditions. A uniform random sampling approach was used to examine the solution space and identify optimal values at local and regional scales. We used a regional sensitivity analysis to examine the effects of parameter correlation and nonuniqueness commonly encountered in multidimensional modeling. The results from this study demonstrate the ability to estimate hydraulic and thermal parameters using measurements of temperature and pressure to simulate exchange and flow paths. Examination of the local parameter space provides the potential for refinement of zones that are used to represent sediment heterogeneity within the model. The results indicate vertical hydraulic conductivity was not identifiable solely using pressure observations; however, a distinct minimum was identified using temperature observations. The measured temperature and pressure and estimated vertical hydraulic conductivity values indicate the presence of a discontinuous low-permeability deposit that limits the vertical penetration of seepage beneath the riffle, whereas there is a much greater exchange where the low-permeability deposit is absent. Using both temperature and pressure to constrain the parameter estimation process provides the lowest overall root-mean-square error as compared to using solely temperature or pressure observations. This study demonstrates the benefits of combining continuous temperature and pressure for simulating hyporheic exchange and flow in a riffle-pool sequence.

Citation: Naranjo, R. C., R. G. Niswonger, M. Stone, C. Davis, and A. Mckay (2012), The use of multiobjective calibration and regional sensitivity analysis in simulating hyporheic exchange, *Water Resour. Res.*, *48*, W01538, doi:10.1029/2011WR011179.

1. Introduction

[2] In the hyporheic zone, surface water infiltrates into the shallow subsurface material forming the channel bed and banks. This water follows the general down-valley gradient, and then returns to the river [*Bencala*, 2011]. In riffle-pool sequences with homogenous sediments, it is commonly understood that river water entering the riverbed at the head of a riffle returns to the river channel at the tail of the riffle near the transition to the pool [*Vaux* 1968; *White*, 1993; *Winter et al.*, 1998]. Flow entering the riverbed can transport organic matter, nutrients, and dissolved oxygen that create environments for biogeochemical processes. Organic matter built up in sediment interstices, referred to as colmation, leads to a reduction of pore volume, consolidation of sediments, and decreased hydraulic conductivity [*Brunke and Gonser*, 1997; *Brunke*, 1999; *Packman and Mackay*, 2003]. The hyporheic zone has been shown to play a crucial role in river management and restoration [*Boulton*, 2007; *Boulton et al.*, 2010], important environments for benthic invertebrates [*Mermillod-Blondin et al.*, 2000; *Franken et al.*, 2001; *Bowker-Davy et al.*, 2006], biochemical reactions [*Franken et al.*, 2001], nutrient cycling and dynamics [*Triska et al.*, 1993; *Dahm et al.*, 1998], and overall ecosystem health [*Valett et al.*, 1994; *Findlay*, 1995; *Brunke and Gonser*, 1997].

[3] Hyporheic flow paths along a longitudinal direction have been shown to be strongly influenced by subsurface heterogeneity, river depth, and river curvature [*Vaux*, 1968; *Harvey and Bencala*, 1993; *Woessner*, 2000; *Cardenas et al.*, 2004] and spacing of bed forms [*Gooseff et al.*, 2006] and morphological features [*Kasahara and Wondzell*, 2003]. In early work, *Vaux* [1968] describes flow patterns that are either diverted back to the surface or forced deeper into the riverbed on the basis of varying riverbed topography and sediment heterogeneity. *Harvey and Bencala* [1993] showed the importance of lateral exchange in gaining conditions. *Storey et al.* [2003] investigated the key factors in controlling hyporheic exchange and showed the dependence of longitudinal and lateral gradients in

[1]Division of Hydrologic Sciences, Desert Research Institute, Reno, Nevada, USA.
[2]U. S. Geological Survey, Carson City, Nevada, USA.
[3]Department of Civil Engineering, University of New Mexico, Albuquerque, New Mexico, USA.
[4]Division of Earth and Ecosystem Sciences, Desert Research Institute, Reno, Nevada, USA.

0043-1397/12/2011WR011179

controlling hyporheic exchange in a riffle pool sequence. *Cardenas et al.* [2004] show the impact of heterogeneity and boundary pressure effect on the shape and depth of exchange. The last two examples highlight the importance of simulating hyporheic exchange at variable temporal and spatial scales and as complex multidimensional heterogeneous systems. Exchange may occur laterally; however, simplifying the model extent to longitudinal 2-D in the thalweg of the channel helps reduce model complexity in defining the boundary conditions and estimating model parameters while simulating exchange along a continuous flow path.

[4] Measuring fluid exchange at the riverbed interface does pose challenges in large river systems. *Kalbus et al.* [2006] describes several methods used in estimating exchange; however, the heat as a tracer method remains popular because of the relatively low cost data loggers and ease of deployment. Since the early applications in ephemeral channels, the heat as a tracer method has been shown to be robust in estimating seepage rates in a variety of river systems, and now has been widely accepted in perennial systems in measuring exchange under both gaining and losing conditions (see reviews by *Stonestrom and Constantz* [2003], *Anderson* [2005], and *Constantz* [2008]). Recent advances in using heat as a tracer include high-resolution synoptic mapping [*Conant*, 2004], thermal imaging [*Loheide and Gorelick*, 2006], and deployment of a distributed temperature sensor [*Day-Lewis et al.*, 2006; *Selker et al.*, 2006]. Several modeling approaches have been developed on the basis of application, conceptualization, and assumptions. Analytical solutions to heat and groundwater flow [*Suzuki*, 1960; *Stallman*, 1963, 1965; *Hatch et al.*, 2006; *Keery et al.*, 2007] have been used extensively for estimating seepage rates. However, these methods are limited to environments with vertical downward flow and sinusoidal temperature fluctuations [*Lautz*, 2010; *Shanafield et al.*, 2011]. Given the assumptions used in analytical solutions, these equations are applicable for vertical seepage, not necessarily hyporheic flow. That is, a hyporheic flow path does not occur in any single direction, rather a flow path tends toward the vertical direction near the riverbed interface and tends toward the horizontal direction beneath the riverbed, such that simulating a flow path requires a multidimensional model.

[5] In heat as a tracer applications, model calibration is typically achieved through manual trial and error methods [*Ronan et al.*, 1998; *Bianchin et al.*, 2010; *Stonestrom and Constantz*, 2003] or using automated parameter estimation techniques [*Bartolino and Niswonger*, 1999; *Niswonger et al.*, 2005]. In both approaches, the calibration procedure is to minimize the differences between observed and simulated temperatures through adjustments of saturated hydraulic conductivity and thermal conductivity that represent a region or zone in the model domain. Typically, the simulated and observed temperatures are compared for the final set of calibrated parameters and parameter sensitivity is determined by manual adjustments to optimal hydraulic conductivity and calculating a percent deviation in seepage [*Bianchin et al.*, 2010]. This sensitivity analysis approach does not consider nonuniqueness and parameter correlation that are typically found in multidimensional systems.

[6] Improvements in model calibration have been made by coupling both temperature and pressure to constrain estimates of hydraulic and thermal properties in evaluating groundwater discharge to rivers [*Doussan et al.*, 1994, *Bartolino and Niswonger*, 1999] and in wetland systems [*Bravo et al.*, 2002]. In a similar coupling approach, solute data and temperature data has been used to estimate transient storage parameters in a multiobjective framework [*Neilson et al.*, 2011]. The use of multiple data types provides great potential for estimating both hydraulic and thermal parameters in hyporheic zone investigations.

[7] Most applications using heat as a tracer to simulate exchange have not considered issues related to nonuniqueness and parameter identifiability. Nonuniqueness can be important in 2-D and 3-D modeling studies because of a greater number of sensitive parameters that need to be estimated during calibration. Because of the multidimensional flow patterns that occur in hyporheic systems, nonunique solutions in hyporheic flow models could also lead to large uncertainty in flux estimates. *Niswonger and Rupp* [2000] estimated the uncertainty in seepage estimates in an ephemeral channel caused by uncertainty in temperature measurements and thermal parameters using a Monte Carlo approach. Through the introduction of error into temperature and thermal parameters, they determined the uncertainty in thermal conductivity had a greater impact on seepage estimates than heat capacity. *Ferguson and Bense* [2011] used stochastic generation of hydraulic conductivity to estimate uncertainty in specific discharge using a one-dimensional approach. They concluded that in areas with relatively high specific discharge and low variance in hydraulic conductivity, the one dimensional approach can provide reasonable results. In areas with greater variance in hydraulic conductivity and specific discharge less than 10^{-7} m s^{-1} will result in lateral flow and greater emphasis in determining the thermal conductivity term [*Ferguson and Bense*, 2011]. These conclusions have important implications for hyporheic investigations where heterogeneity and layering of riverbed deposits create contrasts in hydraulic conductivity, and influence thermal gradients and flow direction.

[8] The uniform random search (URS) Monte Carlo approach is applied to estimate hydraulic and thermal parameters in a two-dimensional (vertical and longitudinal) heat and flow model of a 100 m section of a riffle-pool sequence on the Truckee River, Nevada. Our conceptual model of the subsurface heterogeneity was developed using observed temperature and pressure data to idealize deposits into 3 homogenous zones with different ranges in hydraulic properties. The specific objectives of this work were (1) to develop a flow model that represents hyporheic exchange through a riffle-pool sequence on the basis of continuous temperature and pressure measurements, (2) to evaluate the sensitivity and identifiability of parameters by visual observation of the solution space, (3) to determine the variability in the vertical and horizontal flux rates on the basis of a subset of the model simulations, and (4) to evaluate the relative amount of information provided by temperature and pressure observations. We incorporate principles of model calibration and sensitivity analysis that are typically used for rainfall-runoff model applications.

[9] The modeling approach is used to demonstrate the effectiveness of coupling temperature and pressure measurements to estimate 2-D longitudinal flow through the

hyporheic zone in a riffle-pool sequence. Furthermore, we recognize the importance of nonuniqueness as discussed the literature by the concept of equifinality [*Beven*, 2006], where multiple parameter sets can provide reasonable model results. We incorporate the equifinality concept by examining 5% of the "best" model simulations on the basis of both temperature and pressure to provide qualitative and quantitative examination of the uncertainty in our hyporheic zone modeling. Results are presented according to the RMSE statistic calculated from (1) a regional objective function that includes time series of observations from all observation locations at each zone and (2) a local objective function that only includes time series of observations from a single location. These two objective functions are further divided for further evaluation of model parameters given (1) temperature, (2) pressure, or (3) a combination of both temperature and pressure observations.

2. Site Description

[10] The Truckee River drains from a basin area of 8000 km^2 and encompasses the Sierra Nevada and the Basin and Range physiographic provinces. The river flows over a distance of approximately 184 km from Lake Tahoe to where it terminates at Pyramid Lake (Figure 1a). The study site is located on the lower Truckee River at Little Nixon, located 8 km from the mouth of Pyramid Lake. The precipitation in the Truckee River Basin mainly occurs as snowfall in the higher elevations and reaches the river as runoff or flow through the subsurface.

[11] The riffle-pool sequence at the study area is approximately 20 m wide at the top of the reach and 15 m in the lower section. The depth of flow ranged between 0.20 m in the riffle and 1.3 m in the pool. The discharge at this location is largely controlled by reservoirs and agricultural diversions. The mean monthly flow ranges between 4.81 and 34.55 $m^3\ s^{-1}$ at the USGS gauge 4.5 km upriver of the study area (USGS 10351700 Truckee RV NR Nixon NV). The bed material consists of medium size cobbles and gravels in the riffle and coarse sands to fine silts in the pool area. During low-flow conditions, the right side of the river is very shallow and an alcove of slow moving water forms near P10 and P12 (Figure 1b). The study area was selected because of an up-river point source of nutrients (i.e., a wastewater treatment plant), presence of benthic algae, and its remote location. During periods of low flow, plant respiration and decaying plant material cause incidences of low dissolved oxygen that poses a threat to aquatic ecosystems in the region.

3. Methodology

3.1. Installation and Data Collection

[12] The study area was divided into 6 transects and instrumented with 16 in-river piezometers, and 4 shallow riparian monitoring wells positioned along the riffle-pool sequence. The piezometers were installed to an approximate depth of 1 m beneath the riverbed and were placed perpendicular and parallel to the active channel (Figure 1b). The riverbed topography, river bank and monitoring points were surveyed and referenced to a local control point. The piezometers were constructed of 2.54 cm interior diameter schedule 80 PVC with a 20 cm screened interval starting from 10 cm from the bottom. The monitoring wells were installed within 5 m of the active channel and had screen lengths of 1.5 m. Piezometers were installed by driving a pilot hole using a 3.8 cm diameter metal rod. The rod was extracted by spinning the rod loose using a long pipe wrench for leverage. A 1.27 cm diameter galvanized rod was inserted into the piezometer capped with a Teflon drive tip. To assist with driving force, the top of the metal rod was equipped with a bolt and washers allowing the rod to fit snugly at the top of the piezometer. A posthole driver was used to drive the piezometer to the desired depth, or until refusal.

[13] Seven additional nested minipiezometers (Rapid Creek Research, Boise Idaho) were installed to a depth of 20, 50, 100, and 150 cm below ground surface (bgs) at the riffle head and mid pool locations (NP1–NP7; Figure 1b). The minipiezometers are constructed of stainless steel tubes 0.635 cm diameter with a 3.2 cm welded collar at the top and a drive point welded at the bottom. There were small perforations with a 0.79 mm diameter spaced for 10 cm along the side of the piezometers. The last perforation

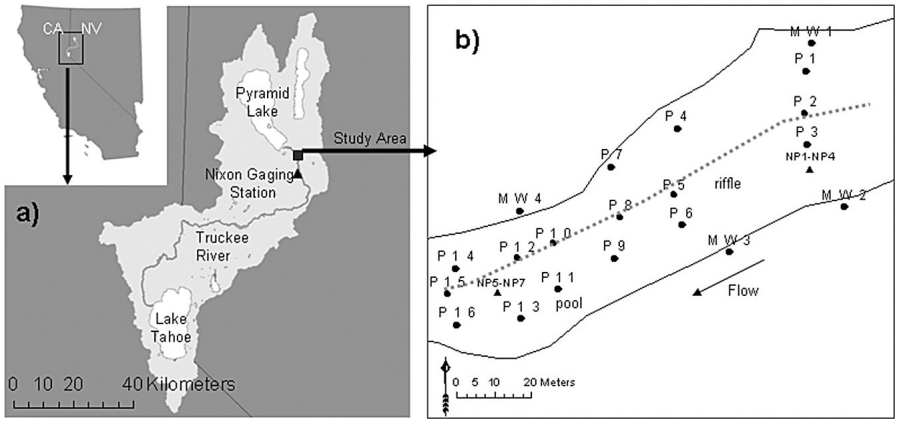

Figure 1. (a) The Truckee River watershed and (b) riffle-pool study area (39.801058°, −119.345166°) showing piezometers (P1–P16), shallow riparian monitoring wells (MW1–MW4), minipiezometers (NP1–NP7), and the longitudinal transect, represented by the dashed line.

was 5 cm from the bottom. The minipiezometers were driven into the riverbed to the desired depth using a sledgehammer.

[14] The monitoring points were equipped with a vertical array of water tight Ibuttons temperature loggers called iBTags (Alpha Mach, Inc.) with an accuracy of $\pm 1.0°C$ and a resolution of 0.125°C. Individual calibration was used to correct and improve the accuracy to $\pm 0.25°C$. The iBtags were attached to a stainless steel wire and placed at two depths, 20 and 50 cm below the riverbed surface. The pressure and temperature near or at 100 cm below ground surface was measured using pressure transducers that were compensated using local barometric pressure measurements.

[15] Continuous stage was recorded along a longitudinal transect at P2, P5, and P15 (Figure 1b) using pressure transducers installed inside 10 cm PVC stilling wells attached to fence posts. Data was measured at 20 min intervals. The piezometers and monitoring wells were sealed with vented caps to prevent surface water from entering during high flows.

[16] Relative water levels between the river and piezometers were used to characterize upwelling and downwelling zones. The vertical hydraulic gradient was calculated: $VHG = \Delta h/\Delta z$, where Δh is the difference in head between the level in the piezometer and level of the riverbed surface and Δz is the depth from the riverbed surface to the midpoint of the screen [*Dahm et al.*, 2006]. The direction of flow is indicated by the sign of the VHG, where negative values are downwelling zones.

[17] Hydraulic conductivity was estimated using falling head tests for comparison to hydraulic conductivity estimated by the URS approach. Hydraulic conductivity was calculated from three repeat falling head tests. For each test, 1 L of river water was poured into the piezometer. Hydraulic conductivity was calculated using the *Bower and Rice* [1976] method [*Halford and Kuniansky*, 2002].

[18] Elevations of the river water surface, water levels in the piezometers and streambed temperatures were measured continuously at 20 min intervals from February–May 2009. Manual periodic water level (monthly to biweekly) measurements in minipiezometers were made from June 2008 to May 2009 using a depth sounder. Surface water levels were converted to pressure head at the riverbed surface and piezometer water levels were converted to pressure head at the midpoint of the screened interval for use in the VS2DH model. Pressure heads will be referred to as simply "pressure" for the remainder of this paper.

3.2. Model Description

[19] The USGS variably saturated two-dimensional hydraulic model VS2DH [*Healy*, 1990; *Healy and Ronan*, 1996; *Hsieh et al.*, 2000] was used to simulate heat and water flow in the hyporheic zone beneath the river. VS2DH, is a two-dimensional (2-D) finite difference model that simulates heat and water flow in variably saturated sediments [*Healy and Ronan*, 1996]. Heat transport is simulated using the advection-dispersion equation and the flow of water is described by the Richards' equation. Model implementation and postprocessing was performed using MATLAB scripts. A 165 m longitudinal cross section along the direction of river flow was used to represent 2-D exchange through the riffle-pool sequence. Along this flow path, river and riverbed temperatures, river stage, and piezometer pressures were monitored continuously from February–May 2009. The model was constructed using hourly time series data from 20 March to 5 May 2009 allowing for an initially stable flow and weather conditions.

[20] Measurements of river temperature and pressure were used to define the variable head and temperature boundary condition along the top of the model domain (Figure 1b). At each surveyed point along the longitudinal transect, the slope of the river surface was linearly interpolated across the longitudinal profile on the basis of continuous stage measurements located at P2, P5, and P14. The pressure along the riffle-pool sequence was then calculated from the slope of the water surface and the elevation of the riverbed from the topographic survey. The left (up-gradient) and right (down-gradient) side boundary conditions were assumed to have a vertical gradient in the range of the nested piezometers (-0.01 m m^{-1}). The placement of the side boundaries were positioned at distal locations to avoid boundary condition effects at internal points in the model, and changes in the head boundaries had only minor effects on pressures in the area of interest. The lower and temperature pressure boundary conditions were linearly interpolated from the side boundary conditions. The grid dimensions were set at uniform spacing with a 0.10 m length in the vertical direction and 3.0 m length in the horizontal direction.

3.3. Parameter Estimation and Sensitivity Analysis

[21] Estimation of hydraulic parameters required by the model is typically achieved through calibration or obtained from literature sources [*Stonestrom and Blasch*, 2003]. Hydraulic conductivity is typically the sole parameter that is adjusted to achieve the "best" match between measured and simulated temperatures and water levels. In this study, a uniform random sampling (URS) approach [*Duan et al.*, 1992; *Beven and Freer*, 2001; *Wagener et. al.*, 2001; *Wagener and Kollat*, 2007] was used estimate hydraulic (vertical and horizontal conductivity) and thermal parameters (thermal conductivity and heat capacity) on the basis of qualitative and quantitative examination of the solution space.

[22] Implementation of the URS method requires the user to specify a region of the parameter space that is considered feasible for a given site on the basis of prior knowledge, such as proxy data or literature values. The upper and lower bounds of the parameter space are then sampled from a uniform probability distribution through Monte Carlo methods. Prior knowledge, in this case separate evaluation of pressure and temperature gradients, suggests that the vertical hydraulic conductivity decreases with depth at the study site. This is likely due to sorting of coarse grain material near the riverbed interface and increased mobility of sediments at high flows. A reduction of vertical hydraulic conductivity from the shallow riverbed to deeper deposits also has been observed in other systems [*Song et al.*, 2007]. On the basis of initial simulations, the upper bound for the shallow hydraulic conductivity (sK_x) was assumed to be 1.0 m h^{-1} and was also defined as the upper bound for all three zones. The ranges in hydraulic and thermal values used in this modeling effort are provided in Table 1. The large negative VHG (> -1.0) and the shape of the temperature envelopes suggested limited exchange at depth in the

Table 1. Summary of Hydraulic and Thermal Parameter Ranges Used in the VS2DH Model[a]

Parameter Description	Symbol	Units	Model Zones			Source
			Shallow	Low Permeability	Deep	
Saturated horizontal hydraulic conductivity	K_x	m h^{-1}	0.1–1.0	0.001–0.01	0.01–1.0	Calibration
Anisotropy	K_z/K_x		0.1–1.0	0.1–1.0	0.01–0.1	Calibration
Saturated vertical hydraulic conductivity	K_z	m h^{-1}	0.01–1.0	1×10^{-4} to 0.01	1×10^{-4} to 0.1	$K_z = K_x (K_z/K_x)$
Porosity	ϕ	m^3 m^{-3}	0.30	0.4	0.30	*Niswonger and Prudic* [2003]
Longitudinal dispersivity	α_L	m	0.5	0.5	0.5	*Niswonger and Prudic* [2003]
Transverse dispersivity	α_T	m	0.1	0.1	0.1	*Niswonger and Prudic* [2003]
Volumetric heat capacity	C_s	J m^{-3} °C^{-1}	1.1–2.5 $\times$ 10^6	1.4 $\times$ 10^6	1.1–2.5 $\times$ 10^6	Calibration
Thermal conductivity of saturated sediments	K_{ts}	W m °C^{-1}	0.5–2.7	1.5	0.5–2.7	Calibration

[a]Parameters in the shallow, low-permeability, and deep zone are noted with prefixes s, lens, and d, respectively.

riffle locations as a result of a lower-permeability deposit between the shallow and deep zones, referred to herein as the low-permeability deposit. This low-permeability deposit could represent a zone of internal colmation [*Brunke*, 1999] or a fine-grained deposit such as a fragipan [*Niswonger and Fogg*, 2008]. The deep zone was assumed to be a transition from highly mobile riverbed deposits to compacted sedimentary deposits with finer-grained material deposited in downwelling riffle zones (P2–P8; Figure 1a).

[23] Although it was hypothesized that a sharp contrast in the permeability was present, we assumed no difference in the upper bound of hydraulic conductivity for the low-permeability deposit and the deep zone. That is, the URS method sampled from a range in hydraulic properties for each of the three zones that did not depend on initial assumption regarding the permeability. We specified 2 orders of magnitude range in vertical hydraulic conductivity for the shallow zone and low-permeability zone and 3 orders of magnitude range in the deep zone (Table 1).

[24] Root-mean-square error (RMSE) values were calculated for each temperature and pressure observation location, referred to as a local RMSE. By observing the local RMSE, variability in optimal parameters for each observation location can provide information about the scale of heterogeneity and the variance in hydraulic and thermal properties. Accordingly, the implementation of the URS method in this study would allow for testing our hypothesis regarding the three zone conceptualization and would provide additional information on the scale of heterogeneity.

[25] One thousand realizations each with different hydraulic and thermal parameters were analyzed, and errors resulting from temperature and pressure estimates were calculated from the root mean square error objective function written as

$$\mathrm{RMSE} = \sqrt{\frac{1}{N}\sum_{t=1}^{N}\left(\sigma_1^{\mathrm{temp,hp}} - \sigma_2^{\mathrm{temp,hp}}\right)^2}, \quad (1)$$

where N is the total number of observations values, σ_1 is simulated temperature or pressure, and σ_2 is observed temperature or pressure. As indicated above, local RMSE was computed for each observation of temperature and pressure independently and a regional overall RMSE was computed by combining all locations of pressure and temperature into a single objective function. For each simulation, the parameters and errors were assumed to be independent of each other. Plotting the model performance (RMSE) against each parameter provides a means to determine identifiable parameters, referred to herein as a "RMSE scatterplot." Parameters are identifiable if a distinct minimum in the RMSE is present, whereas unidentifiable parameters exhibit similar RMSE values for a range in the parameter values. In VS2DH, horizontal hydraulic conductivity (K_x) and anisotropy (K_z/K_x) are model inputs, while vertical hydraulic conductivity (K_z) is calculated by taking the product of the two (Table 1). The range used for anisotropy (Table 1), reflects the assumption that K_x is greater than K_z. This assumption was supported by initial simulated results. The model was allowed to "warm up" for 124 h period where simulated values were not used to calculate the objective function.

[26] Parameter sensitivity was determined using a global method called regional sensitivity analysis (RSA) [*Young*, 1978; *Hornberger and Spear*, 1981; *Freer et al.*, 1996; *Wagener et al.*, 2001]. The method, as modified by *Wagener et al.* [2001], divides the population of transformed objective functions into 10 groups of equal size, ranked by their performance and plotted against the feasible parameter range. Sensitive parameters are identified by large differences between the cumulative normalized distributions (CND) for each group. If the objective function is insensitive to a particular parameter then the CND will have a relatively small slope over the range of the parameter value, whereas sensitive parameters will have a steep slope [*Wagener et al.*, 2001]. When used together, the scatter and RSA plots provide a means to illustrate the identifiability and evaluation of model parameters and for refinement of parameter ranges and estimation of model uncertainty [*Wagener et al.*, 2001; *Wagener and Kollat*, 2007].

4. Results

4.1. Field Observations

[27] Two major events, with contrasting river temperatures, occurred during the monitoring period on 20 April 2009 (11 m^3 s^{-1}) and 3 May 2009 (46 m^3 s^{-1}) that resulted in a doubling and an order-of-magnitude increase in discharge, respectively (Figure 2a). The discharge during the initial monitoring period was relatively constant with an average of 5.5 m^3 s^{-1} and a 2.8°C diel temperature variation (Figure 2a). The discharge event that occurred on 20 April occurred during a period when ambient temperatures

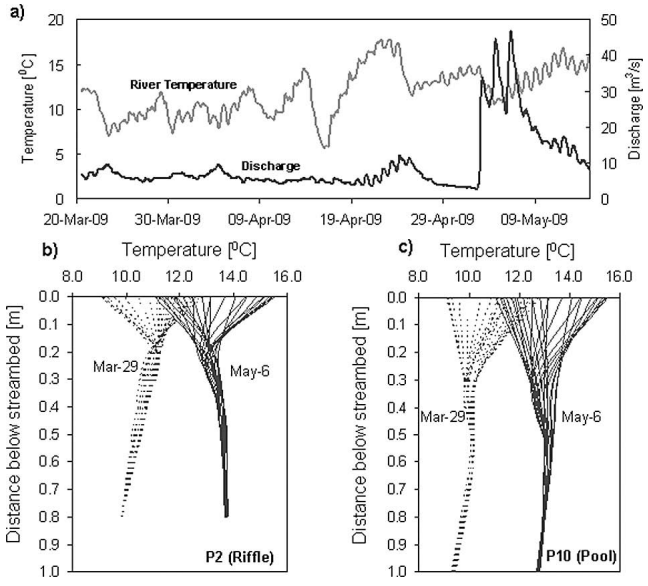

Figure 2. (a) Truckee River temperature (gray line) and discharge (black line) during the simulation period. Discharge was measured from U.S. Geological Survey gage 10351700, TRUCKEE RV NR NIXON, NV. Vertical temperature envelopes were measured during a 24 h period at low-flow (5.9 m^3 s^{-1}; 29 March 2009) and high-flow (46.5 m^3 s^{-1}; 6 May 2009) periods at the nested piezometers located in the (b) riffle and (c) pool locations.

were increasing and relatively warmer discharge from the river infiltrated into a cooler riverbed. The average river temperature was 10°C during the relatively steady flow that occurred between 20 March and 14 April. The river temperatures steadily increased from 5.3°C to 17.1°C from 16 to 20 April. The second discharge event on 3 May resulted in a 3.0°C decrease in river temperature. At this point, the river began to exhibit a diel temperature variation of 2.8°C between 6 and 13 May, with an average river temperature of 10.2°C on 13 May (Figure 2a). During both discharge events, the river temperature was relatively warmer than the riverbed.

[28] Temperature envelopes can be used qualitatively to assess the relative amount of river seepage that penetrates into the deeper sediment (>1 m beneath the riverbed). *Lapham* [1989] showed that for downward seepage rates, seasonal temperature envelopes will be broad several meters beneath a river. Similarly, this concept can be used to look at diel temperature envelopes. Temperature envelopes measured beneath the riffle (upriver) sections of the Truckee River indicate that seepage is impeded above a depth of 1 m with an extinction depth near 0.20 m (Figure 2b). These temperature envelopes combined with the large VHG measured at the shallow and deep piezometers beneath the riffles indicate that there is a low-permeability zone between the shallow and deep observations beneath the riffles that does not extent beneath the pool (Figure 2c).

[29] Longitudinal patterns of VHG measured from the top of the riffle to the end of the pool show the deviation from downward vertical flow to upward vertical flow typified by riffle-pool conceptual models (Figure 3a). At the head of the riffle, locations P1–P6 were predominantly downwelling with a greater variation in VHG, suggesting a greater sensitivity to changes in stage. In pool locations P10–P15, the gradient is near zero with occasional periods of slightly upward flow (Figure 3a).

[30] The VHG determined from nested wells reveal greater detail of the complex flow directions in the riverbed as compared to VHG typically measured between the river and a single piezometer. The VHGs show the change in gradient from downward to neutral or horizontal flow in the NP1–NP4 piezometers located on the head of the riffle (Figure 3b). VHGs calculated using the river water surface and the deepest piezometer water levels are much different than VHGs calculated using the shallow and deep piezometer water levels, illustrating a greater variability in flow directions beneath the riverbed (Figure 3c). In the pool, the vertical gradients measured at NP5–NP7 suggest upward flow (Figure 3d), and significant variability in the VHG with depth (Figure 3e). The variation in flow direction (positive or negative VHG) between each nested piezometer

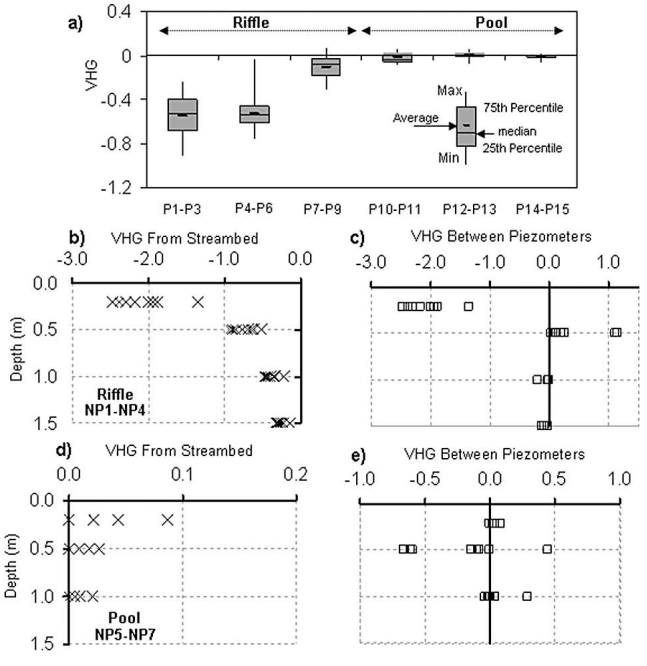

Figure 3. (a) Vertical hydraulic gradient (VHG) as a function of location and depth (b, d) below the streambed referenced from the streambed and (c, e) between nested piezometers located at head of the riffle and middle of the pool from periodic measurements (8–9 June). The VHG measured across each transect (Figure 3a) show upwelling and downwelling zones as measured from the streambed surface to the screened interval at each piezometer. The VHG measurement between piezometers (Figures 3c and 3e) reflect more complex flow patterns because of smaller-scale heterogeneity as compared to gradients averaged from the streambed (Figures 3b and 3d). Positive, zero, or negative VHG suggest the potential flow direction is the upwelling, horizontal, or downwelling direction, respectively. Scale on horizontal axis was modified to emphasize measured values.

confirms the existence of multidirectional flow patterns and using single depth measurements to infer direction should be used with caution.

[31] Hydraulic conductivity estimated from falling head tests (K_{slug}) of in-river piezometers ranged from 0.003–2.016 m h^{-1}, with a geometric mean of 0.17 m h^{-1}. At most locations, the head elevations recovered to equilibrium conditions within 5–25 s. Falling head tests were not performed in nested piezometers because of the inability to reliably measure head changes.

4.2. Model Calibration and Sensitivity Analysis

[32] Measured temperatures and pressures were used to calibrate VS2DH on the basis of a conceptual model of the riffle-pool hyporheic zone that incorporated three distinct zones with differing hydraulic and thermal properties. The conceptual model was defined by a shallow zone, a low-permeability zone, and a deep zone (Figure 4).

[33] Figure 5 shows the results of the model performance and parameter identifiability on the basis of a regional pressure (PRMSE) and temperature (TRMSE) for all shallow and deep zones given parameters K_x, K_z, and K_{ts}. The optimal value is shown as a diamond in Figure 5, as determined by the lowest RMSE. Unique solutions can be determined visually by evaluating the shape and distribution of the RMSE scatter points at the optimal solution. As stated above, parameters are identifiable if a distinct minimum in the RMSE is present, whereas unidentifiable parameters exhibit similar RMSE values for a range in the parameter values. The optimal values for the horizontal hydraulic conductivity sK_z (shallow) and dK_z (deep) were not identifiable on the basis of pressure (PRMSE) but a distinct minimum was identified with temperature (TRMSE). The scatterplots for sK_z and dK_z given PRMSE revealed similar results (not shown). For sK_z and dK_z (PRMSE), sK_{ts} and dK_{ts} (TRMSE), the values that resulted in the minimum RMSE were near the minimum value in the assigned ranges (Table 1). The sK_z, dK_z, dK_x, parameters were slightly more identifiable than others with a distinct value corresponding to a minimal regional objective function (Figure 5).

[34] Figure 6 shows the RSA plots for the same parameters, where the optimal performing group is shown by the black line. The parameter population is split into 10 groups of equal size and the cumulative distribution of the parameters in each group is plotted. As shown by the slope of the CND for each bin, the sensitivity the parameter depends on its location in the solution space (i.e., the values of other variable parameters in a simulation). The sensitivity of sK_z and dK_z is considerably higher near the minimum range of the parameters, as defined by values of PRMSE. However, the sensitivity of sK_{ts} is high over the complete range of the parameter values, as defined by values of TRMSE. Overall, there are similarities between the identifiability determined by the RMSE scatterplots in Figure 5 and the sensitivity determined by visualization the RSA plots.

[35] Evaluation of model performance on the basis of measured temperatures in the shallow and deep riffle and pool locations are shown in Figures 7 and 8. For brevity, only parameters K_x and K_z are shown. The differences between the individual location (local) RMSE values and the overall RMSE values are illustrated by the solid circle and the open diamond, respectively. At P10 (screened at a depth of 20 cm), the local optimal value of sK_x was identifiable (0.24 m h^{-1}), but different than the value determined by the overall TRMSE (1.0 m h^{-1}). However, the K_x was less identifiable in the shallow than the deep zone. At other shallow locations (i.e., P2, P12, and P15), the sK_x was different, but not significantly different between the local and overall RMSE. At all deep locations, the parameters dK_x and dK_z are identifiable on the basis of TRMSE but not

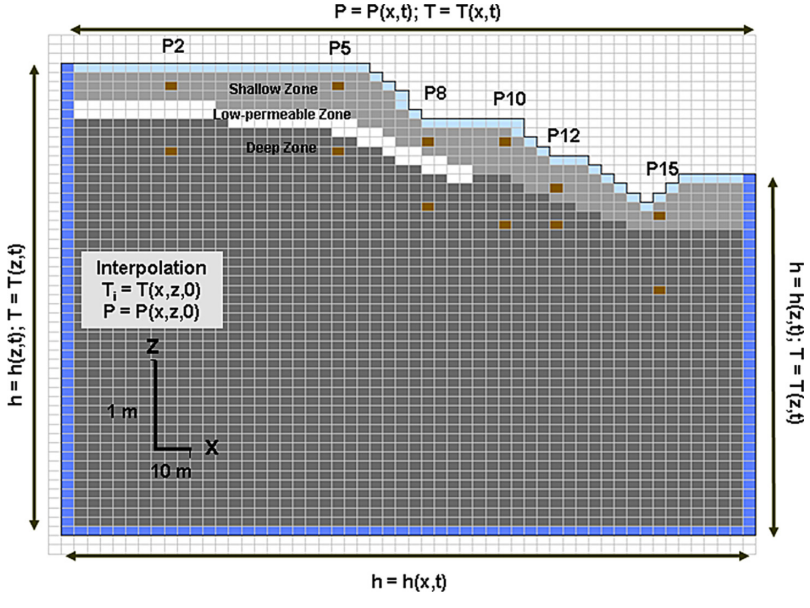

Figure 4. Location of model layers, grid, boundaries, and observations for the VS2DH model. Grid dimensions are 3.0 × 0.10 m, and domain is 160 m in length. Drawing is scaled 1:20, and flow direction is from east to west. P is the pressure (m), T is temperature (°C), and x and z are distance (m) along the horizontal and vertical dimensions, respectively.

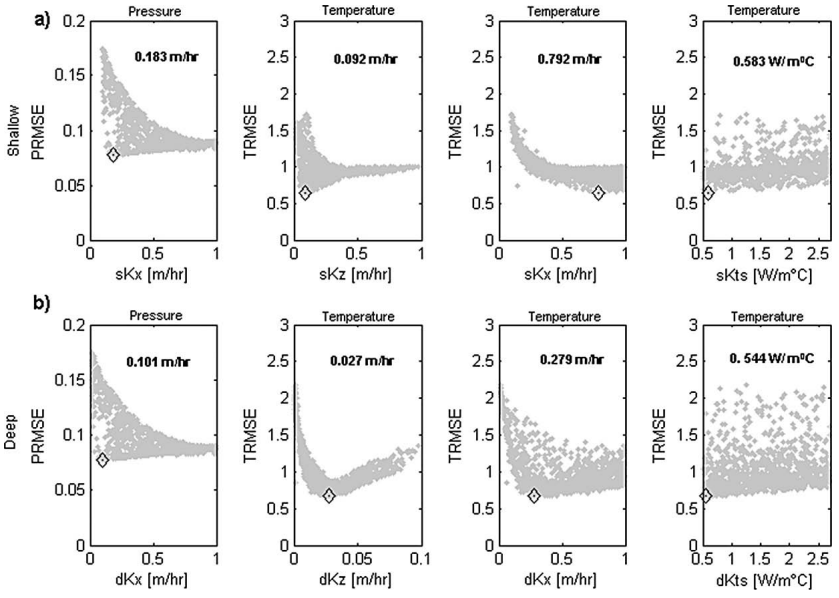

Figure 5. Scatterplots showing parameter identifiability for the (a) shallow and (b) deep zones predicted by a regional overall root-mean-square error (RMSE) for pressure (PRMSE) and temperature (TRMSE). Each scatter point correspond to 1 of 1000 VS2DH simulations. The diamond corresponds to the optimal value identified by the lowest RMSE. Parameter values near the origin reflect parameter values estimated at the minimum of the parameter range. Horizontal hydraulic conductivity (K_x), vertical hydraulic conductivity (K_z), and thermal conductivity (K_{ts}) are shown for the shallow and deep zones, denoted by prefixes s and d, respectively.

identifiable on the basis of PRMSE. As shown in Figure 5, the vertical and horizontal hydraulic conductivity determined by PRMSE was not identifiable within the range of values initially assigned.

[36] Table 2 summarizes the hydraulic and thermal parameters for each observation estimated on the basis of the local RMSE values. The hydraulic conductivity values estimated by slug tests (K_{slug}) were in general agreement with values

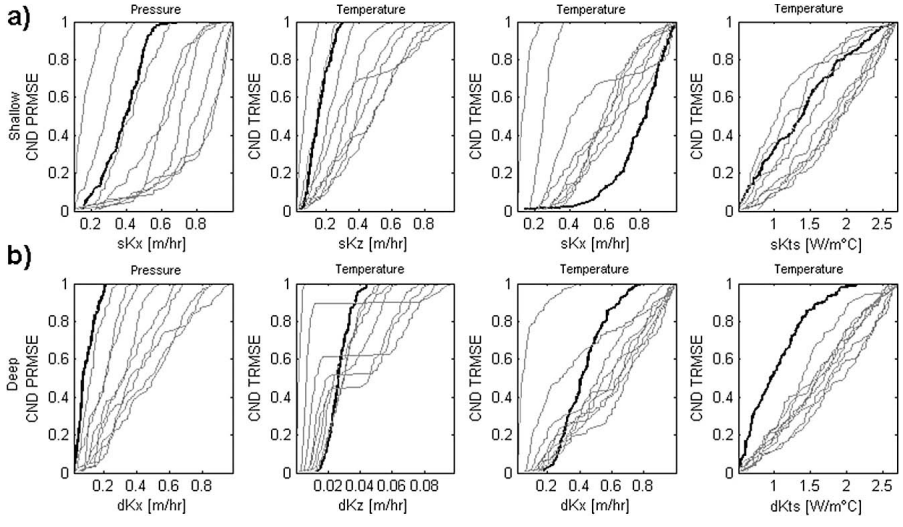

Figure 6. The regional sensitivity analysis plots showing the sensitivity of model parameters plotted across the feasible parameter range for the (a) shallow and (b) deep zones. The parameters are ranked according to the objective function, divided into 10 bins of equal size, and normalized so each bin sums to unity, and the cumulative distribution for each bin is plotted versus the parameter value. The black line corresponds to the bin of the parameters with the best performing model simulations. Parameter sensitivity can be assessed by the spread between each of the 10 bins and the slope of the distribution. Higher spread in each of the bins and a steep slope correspond to higher sensitivity. Horizontal hydraulic conductivity (K_x), vertical hydraulic conductivity (K_z), and thermal conductivity (K_{ts}) are shown for the shallow and deep zones, denoted by prefixes s and d, respectively.

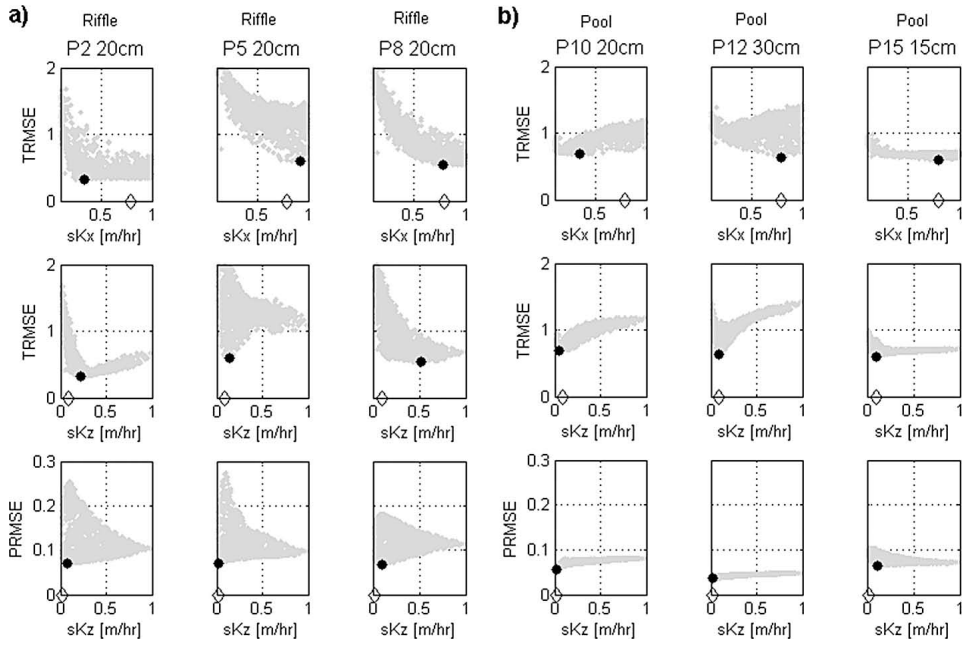

Figure 7. Scatterplots of model performance at the (a) riffle (P2–P8) and (b) pool (P10–P15) locations in the shallow zone. Each scatter point corresponds to 1 of 1000 VS2DH simulations. The solid circle corresponds to the parameter value with the lowest local RMSE, whereas the diamond corresponds to the parameter value given the regional RMSE. Parameter values near the origin reflect parameter values estimated at the minimum of the parameter range. (top) Shallow horizontal hydraulic conductivity (sK_x) and (middle) vertical hydraulic conductivity (sK_z) determined by temperature RMSE (TRMSE), respectively. (bottom) The shallow vertical hydraulic conductivity (sK_z) determined by pressure RMSE (PRMSE) shown for comparison to TRMSE in Figure 7 (middle).

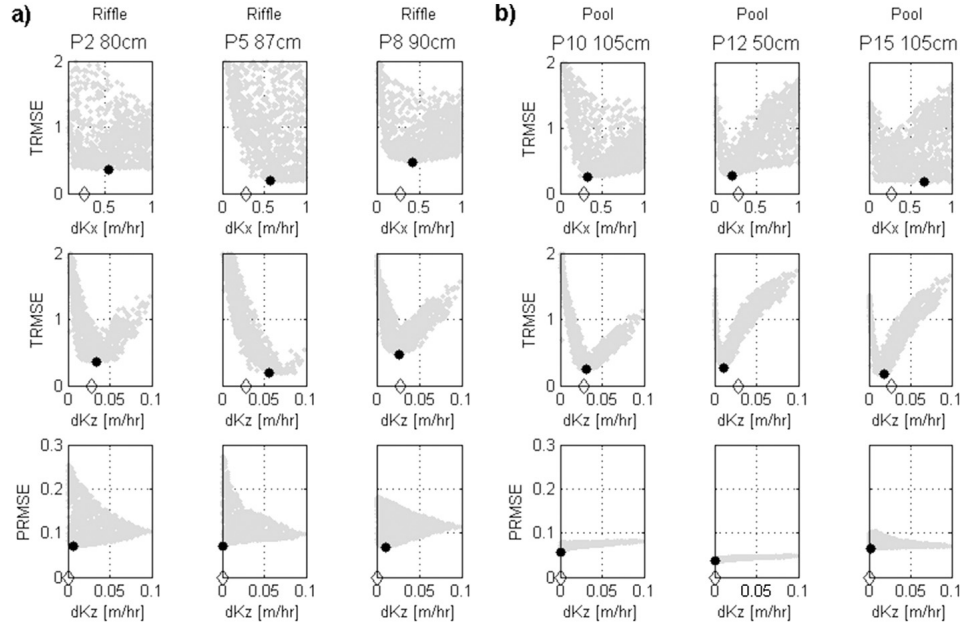

Figure 8. Scatterplots of model performance at (a) riffle (P2–P8) and (b) pool locations (P10–15) in the deep zone. Each scatter point corresponds to 1 of 1000 VS2DH simulations. The solid circle corresponds to the parameter value with the lowest local RMSE, whereas the diamond corresponds to the parameter value given the regional RMSE. Parameter values near zero reflect parameter values estimated at the minimum of the parameter range. (top) Deep horizontal hydraulic conductivity (dK_x) and (middle) vertical hydraulic conductivity (dK_z) determined by temperature RMSE (TRMSE). (bottom) Deep vertical hydraulic conductivity (dK_z) determined by pressure RMSE (PRMSE), shown for comparison to TRMSE in Figure 8 (middle).

Table 2. Thermal and Hydraulic Parameters Derived From the VS2DH Model for Each Location Along the Riffle-Pool Sequence Based on Local TRMSE[a]

Location	K_{slug} (m h^{-1})	sK_{ts} (W m^{-1} °C^{-1})	sC_s (J m^{-1} °C^{-1})	sK_x (m h^{-1})	sK_z (m h^{-1})	dK_{ts} (W m^{-1} °C^{-1})	dC_s (J m^{-1} °C^{-1})	dK_x (m h^{-1})	dK_z (m h^{-1})
P2	0.097	0.90	1.2×10^6	0.70	0.19	1.38	2.4×10^6	0.98	0.05
P5	1.854	0.50	1.3×10^6	0.99	0.10	2.68	2.0×10^6	0.37	0.04
P8	0.272	1.52	1.2×10^6	0.98	0.51	1.55	2.3×10^6	0.25	0.01
P10	0.310	0.51	1.3×10^6	0.29	0.03	2.42	1.2×10^6	0.26	0.02
P12	0.003	0.55	1.3×10^6	0.83	0.08	2.44	2.5×10^6	0.07	0.01
P15	0.468	0.50	1.3×10^6	0.83	0.08	0.86	2.0×10^6	0.45	0.01

[a]Prefixes s and d represent shallow and deep locations, respectively. Subscripts x and z represent horizontal and vertical discretization, respectively. Hydraulic conductivity was estimated by slug test (K_{slug}). TRMSE, root-mean-square error for temperature.

estimated using the RSA approach at the deep locations (i.e., P8, P10, and P15). The thermal conductivity (K_{ts}) was lower overall in the shallow zone (0.50 to 1.52 W m^{-2} °C^{-1}) than in the deep zone (0.86 to 2.68 W m^{-2} °C^{-1}). The heat capacity (C_s) was greater in the deeper zone than in the shallow zone.

4.3. Simulated Temperature and Pressure

[37] The URS method provides a means of identifying the optimal set of parameters according to the overall RMSE value. Additionally, the top 5% of solutions (i.e., parameter sets that result in the lowest 5% RMSE values) provides a means of evaluating the uncertainty of model simulations. Figure 9 shows the observed and simulated temperatures for shallow and deep locations. Overall, there is close agreement between observed and simulated temperatures for the top 5% RMSE solutions; with approximately 1.0°C bias at locations P5 20 cm and P8 20 cm. The model tends to over estimate the diel oscillations at shallow pool location P15 20 cm, suggesting there is heterogeneity at this location that is not included in the model. However, inclusion of additional heterogeneity likely would result in less identifiable parameters, which expresses the subtle balance between accuracy and uniqueness. The model captures the long-term thermal signal in the deep observations. Figure 10 shows the observed and simulated pressures. The model simulated a greater variation of pressures in the riffle locations than in the pools because of the low-permeability zone between the shallow and deeper zones. Generally, the observed pressure behavior mimicked the behavior of the river stage. The model captured the thermal and pressure behavior indicated by the agreement between the observed and simulated results (Figures 9 and 10).

4.4. Simulated Flux Rates and Flow Paths

[38] Figure 11 shows the simulated vertical flux rates in the riffle and pool locations. Negative flux in the vertical direction (q_z) represents flow in the upward direction. For brevity, only the vertical flux rates are shown. The simulated flux in the shallow locations P8 20 cm and P12 30 cm are in the upward direction. The other locations are predominantly in the downward direction. The first flow event (20 April) and second flow (3 May) event occurred during simulation times 600 and 920 hours, respectively. The

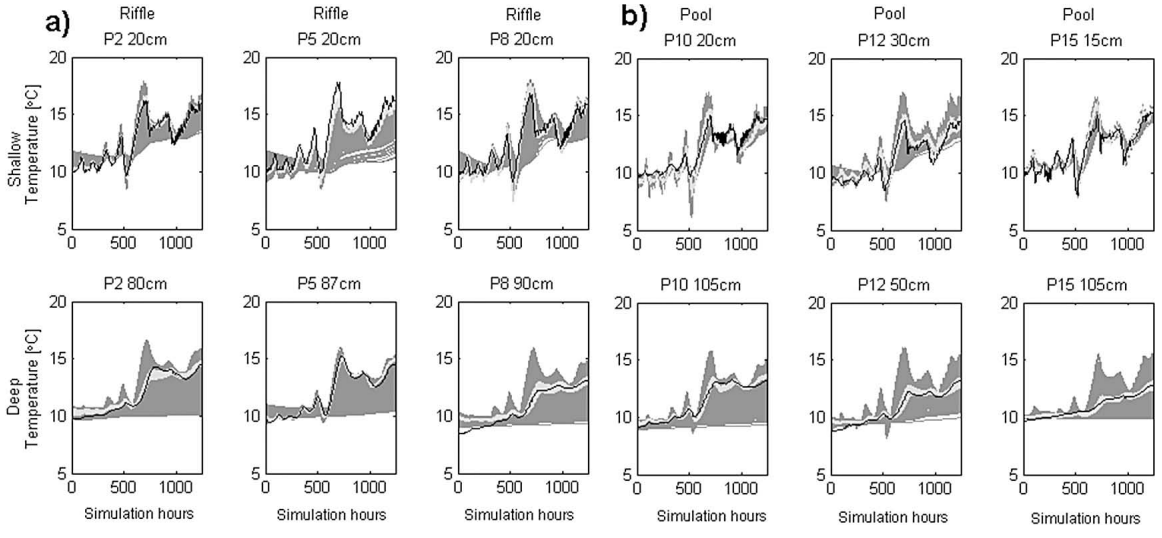

Figure 9. Observed (black line) and simulated streambed temperatures showing all realizations (dark gray shading) and the "best" 5% (light gray shading) based on overall RMSE at the (a) riffle (P2–P8) and (b) pool (P10–P15) (top) shallow and (bottom) deep zone locations. The simulation period is from 20 March 2009, 13:00 LT, to 15 May 09, 15:00 LT. The first flow event (20 April) and second flow event (3 May) occurred during simulation times 600 and 920 hours, respectively.

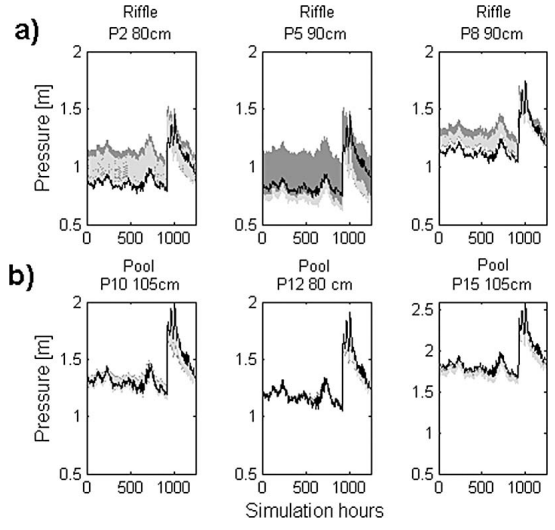

Figure 10. Observed (black line) and simulated head pressure showing all realizations (dark gray shading) and best 5% (light gray shading) based on the overall RMSE for the (a) riffle and (b) pool locations. The greater variation in simulated pressure at the riffle locations is due to the uniform random search method applied to the low-permeability zone that does not extend into the pools. The simulation period is from 20 March 2009, 13:00 LT, to 15 May 2009, 15:00 LT. Pressure was measured near the screened interval within the deep zone. The first flow event (20 April) and second flow event (3 May) occurred during simulation times 600 and 920 hours, respectively.

response of each event on the vertical flux was variable depending on location and direction of flux. Generally, the increase in river flow resulted in increases in vertical flux through the riverbed surface. The simulated flux at location P10 (shallow and deep) exhibited a slight flow decrease or suppression of upward flow because of the increased stage in the river.

[39] Figure 12a shows the simulated vertical flux across the riverbed interface for both low flow (29 March) and high flow (6 May). The effect of the low-permeability zone in the riffle area can be seen by the lower estimated vertical downward flux (1.0×10^{-4} to 3.0×10^{-4} m h^{-1}). Most of the exchange in both the upward and downward direction occurs where the low-permeability zone becomes discontinuous, just upriver of the pools. The 6 May flow event (flow increased from 5.9 to 46.5 m^3 s^{-1}) increased the vertical upward flux just downriver of P10 by an order of magnitude (flux increased from 9.0×10^{-4} to 4.2×10^{-3} m h^{-1}). At an adjacent downward flow path (near P12), the flux increased from 1.0×10^{-3} to 3.9×10^{-3} m h^{-1} because of the 6 May flow event (Figure 12a).

[40] Figure 12b shows the simulated temperatures and idealized flow patterns for the flow event that occurred on 6 May. The steep thermal gradient and horizontal seepage caused by the low-permeability zone is clearly identified in the shallow riffle section of the study area (P2–P8). The areas with the greatest exchange with the river occur at short flow paths at the transition from lower riffle to pool near P8. Downward seepage at the upper section of the riffle near P2 is predominantly downward and horizontal. In the pool, there is greater exchange with the river because of relatively short flow paths (Figure 12b). Smaller-scale flow paths in the pool area appear to have the greatest exchange with the river in low- and high-flow conditions. Table 3 summarizes the average horizontal and vertical flux rates.

[41] Using temperature and pressure observations to constrain the parameter estimation process provides the lowest overall RMSE as compared to using temperature or pressure observations alone. Table 4 summarizes the "best" parameter values resulting from the single objective function

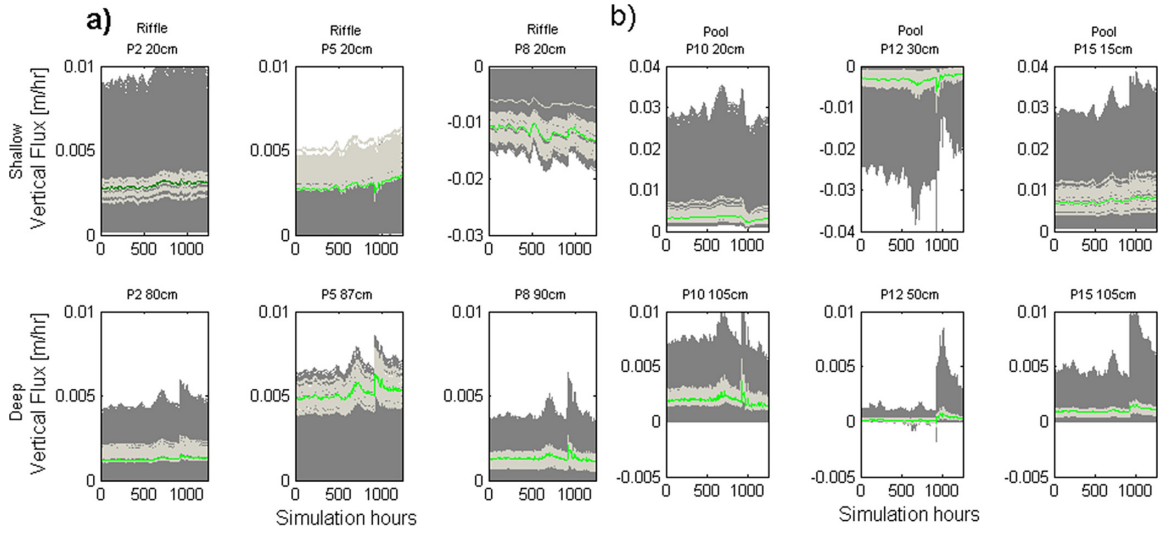

Figure 11. Simulated vertical and horizontal flux at the (a) riffle and (b) pool locations for the (top) shallow and (bottom) deep zones. All realizations (dark gray shading) and best 5% (light gray shading) and 2.5% (green shading) are based on the overall RMSE. Negative flux in the vertical direction represents flow in the upward direction. The simulation period is from 20 March 2009, 13:00 LT, to 15 May 2009, 15:00 LT. The first flow event (20 April) and second flow event (3 May) occurred during simulation times 06:00 and 09:20 LT, respectively.

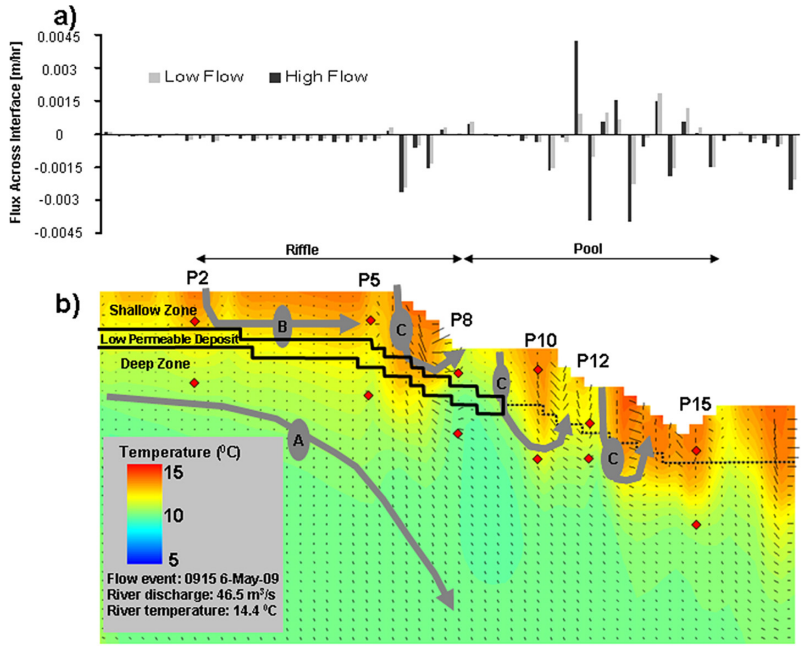

Figure 12. (a) Vertical flux across the streambed interface at low flow (5.9 $m^3\ s^{-1}$; 29 March 2009, 13:00 LT) and high flow (46.5 $m^3\ s^{-1}$; 6 May 2009, 09:15 LT) showing the effect of the low-permeability deposit, streambed slope, and flow path direction on magnitude of exchange. (b) Simulated streambed temperatures, idealized flow paths (gray lines), observations (red diamonds), and velocity vectors during the peak discharge of 46.5 $m^3\ s^{-1}$ and temperature of 14.4°C on 6 May 2009. Deep flow path (labeled A), shallow horizontal flow path (B), and short upwelling flow path (C) in the riffle and pool section are in a predominantly losing system. The dashed line represents the boundary between upper and lower deposits.

measure for temperature (TRMSE) and pressure (PRMSE) and combined RMSE. The horizontal and vertical hydraulic conductivity estimated by temperature and combined temperature and pressure are very similar where as the parameters estimated from pressure alone can be an order of magnitude lower (sK_z, dK_z, lens K_z). For the single objective function (TRMSE and PRMSE), the vertical hydraulic conductivity for the upper (sK_z), low-permeability (lens K_z), and deep (dK_z) zones is 0.22, 0.0019, and 0.018 m h^{-1}, respectively. Given a single objective function, the parameters set provided by the temperature was in close approximation to the combined pressure and temperature objective function.

Table 3. Average Horizontal and Vertical Fluxes at the Riffle and Pool Locations[a]

Location	sq_x (m h^{-1})	sq_z (m h^{-1})	dq_x (m h^{-1})	dq_z (m h^{-1})
P2	4.9×10^{-3}	-3.0×10^{-3}	2.1×10^{-3}	-1.3×10^{-3}
P5	3.9×10^{-3}	-2.9×10^{-3}	8.2×10^{-3}	-5.2×10^{-3}
P8	1.3×10^{-2}	1.2×10^{-2}	6.5×10^{-3}	-1.3×10^{-4}
P10	5.6×10^{-3}	-3.3×10^{-3}	9.5×10^{-3}	-1.9×10^{-3}
P12	1.8×10^{-2}	3.1×10^{-3}	2.8×10^{-3}	-1.9×10^{-4}
P15	1.1×10^{-2}	-7.3×10^{-3}	7.2×10^{-2}	-1.0×10^{-3}

[a]Prefixes s and d represent shallow and deep locations, respectively. Subscripts x and z represent horizontal and vertical discretization, respectively. Negative values of sq_z correspond to the downwelling direction.

5. Discussion

[42] The VHG can vary significantly when compared to vertically integrated measurements. Measurements at the fine scale (<1.0 m) were able to identify the effects of subsurface heterogeneity on flow direction. Although the VHG data measured along the longitudinal profile confirm earlier conceptual models of riffle-pool hyporheic flow, more complex flow patterns emerge at the finer scale through both measurements and modeling (Figures 3c, 3e, and 12). These findings are similar to those of *Käser et al.* [2009], whose continuous monitoring of VHG indicates nonlinear behavior with respect to stage at riffle and pool locations, and by *Lautz et al.* [2010], who identified smaller-scale heterogeneity through modeling that was not evident through VHG measurements taken at one depth. The VHG data appeared to confirm conclusions drawn from the temperature envelops and low diel amplitude temperature signal at depth; a low-permeability ($K_x = 4.0 \times 10^{-3}$ m h^{-1}; $K_z = 1.9 \times 10^{-3}$ m h^{-1}) zone about 0.30 m below the riverbed is enhancing horizontal flow at the riffle section of the study site. Therefore, the use of vertically nested temperature and VHG measurements provides valuable information for inferring flow direction, assigning hydraulic conductivity and boundary conditions for heat as a tracer modeling.

[43] The use of continuous temperature and pressure data provided valuable information for developing a conceptual flow model of the hyporheic zone. We defined the subsurface heterogeneity on the basis of contrasts in VHG,

Table 4. Summary of Hydraulic Conductivity for the Three Zones Estimated From Temperature, Head Pressure, and Combining Temperature and Head Pressure for Single Objective Measures TRMSE, PRMSE, and Regional Overall RMSE[a]

	TRMSE	PRMSE	Regional Overall RMSE	sK_x (m h^{-1})	sK_z (m h^{-1})	Lens K_x (m h^{-1})	Lens K_z (m h^{-1})	dK_x (m h^{-1})	dK_z (m h^{-1})
Temperature	0.72	0.091	1.63	0.47	0.29	0.006	0.0039	0.42	0.026
Pressure	1.61	0.077	2.38	0.18	0.02	0.001	0.0001	0.10	0.001
Combined	0.74	0.083	1.57	0.50	0.22	0.004	0.0019	0.45	0.018

[a]PRMSE, root-mean-square error for pressure.

pressure and temperature gradients. We tested the conceptual model by allowing the hydraulic conductivity to range across an order of magnitude for the between the shallow, low-permeability, and deep zones. The optimal hydraulic and thermal properties of the riverbed were estimated by examining solution space through the use of single and multiple objective functions. On the basis of pressure alone, the shallow hydraulic conductivity was nonunique (RMSE values that are insensitive to parameter values) and unidentifiable. Inspection of the RMSE scatterplots for TRMSE and PRMSE revealed a trade-off between individual objectives, showing that no single solution existed that produced the lowest RMSE for all observation locations. This was expected on the basis of the results of previous studies that have come to similar conclusions using multiobjectives [*Doussan et al.*, 1994; *Bravo et al.*, 2002; *Neilson et al.*, 2011]. However, the local optimal parameter values were relatively consistent with the overall optimal parameter values, indicating that the most influential controls on seepage were represented in the model (Table 2).

[44] Pressures alone did not provide identifiable estimates of hydraulic parameters, as shown by the variability of error at the optimal solution (Figures 5, 7, and 8). Temperature observations provided greater information than pressure measurements, allowing for the hydraulic properties to be more identifiable, as illustrated by the distinct minimum value of the RMSE. Closer examination of the normalized parameters for the 5% of the "best" model simulations determined by temperature, pressure, and the combination of the two are shown in Figure 13a. A zero value of the normalized parameter indicates the value is equal to the lower bound of the predefined range. The wide spread in parameter values indicate the high degree of uncertainty and equifinality [*Beven*, 2006]. The model parameters given by pressure are outside of the 5% "best" solutions. More pronounced was the inability of pressure to identify sK_z, dK_z, lens K_x, and lens K_z. The optimal parameters were identified at the minimum value for each range. In the deeper zone, parameters dKz and dK_x was more identifiable with unique solutions identified by the scatter of the RMSE, and an optimal solution.

[45] Incorporating continuous pressure measurements provided additional constraint on the estimates of vertical and horizontal hydraulic conductivity. This approach can be further advanced by using optimization techniques [*Duan et al.*, 1992; *Vrugt et al.*, 2003] for determining the optimal values based on compromises or trade-offs in a single or multiobjective framework (Figure 13b). The trade-off between two objective functions is commonly described as the "Pareto solutions" and in the absence of model and measurement error, a unique set of parameters that simultaneously describes the observed data would be found. It is important to note, however, that combining pressure and temperature observations into a single objective function without closer examination of solution space for each observation may result in bias in model performance and loss of information at each observation. Evaluation of the solution space can help reduce the range of parameters or help identify heterogeneity in riverbed deposits. The use of pilot point regularization [*Doherty*, 2003] to automate the spatial structure of the hydraulic conductivity field coupled with calibration might help overcome the subjectivity and challenge in defining the level of heterogeneity within the model domain.

[46] The RSA results indicate that the model response was more sensitive to changes in hydraulic parameters

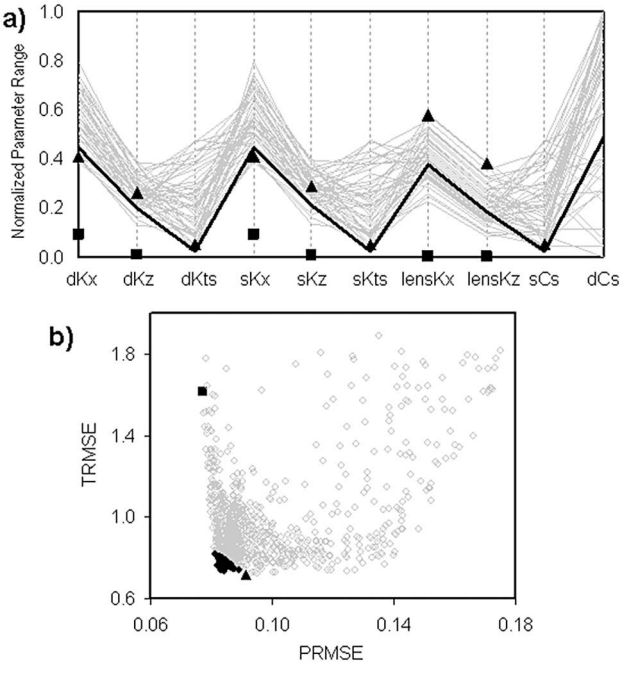

Figure 13. (a) Normalized parameter space for parameter values identified by optimal values for temperature (triangles), pressure (squares), and combining both pressure and temperature RMSE (black line) among 5% of the best solutions (gray lines) for overall RMSE. Each line represents one of the parameter sets. Thermal parameters dK_{ts}, sK_{ts}, sC_s, and dC_s determined from pressure are not shown. (b) Multiobjective plot showing the trade-off between the temperature and pressure RMSE for all model runs. The best model simulations represented by 5% of the better performing model simulations ranked by the regional overall RMSE (black) and the lowest overall pressure and temperature RMSE are shown.

when using temperature observations relative to pressure observations. The model parameters are more sensitive within the optimal solutions as shown by the steeper slope of the cumulative normalized distribution for sK_z and dK_z for both temperature and pressure. However, for pressure the optimal sK_z is less identifiable. The URS and RSA results suggest a lower range of values for sK_{ts} and dK_{ts} may have been necessary to identify unique parameter values. The dK_{ts} and sK_x parameters were not sensitive within the overall RMSE; however, closer evaluation of the location specific RMSE and RSA results revealed a greater sensitivity and identifiability of parameters. Thus, the application of a multiobjective approach should also include evaluation of the solution space at each observation and a subsequent localized sensitivity analysis (RSA). Further, examination of local RMSE values provides information about how heterogeneity affects flow and heat transport in the riverbed. If model parameters identified at the local scale were found to be significantly different from the regionally inferred parameters, additional zones would have been used around the observed locations. However, defining the spatial extent of the additional zone or zones would be subjective and may result in inducing errors to other locations within the model domain. Given the regionally identified parameters did not significantly differ from the local scale; we feel the three zone conceptualization provided a good representation of the heterogeneity for the study area.

[47] Fine-grained sediment or organic matter deposited into the riverbed in the downwelling zones may have resulted in lower-permeability deposits impeding vertical seepage beneath the river and may be contributing reduction of thermal conductivity. The thermal conductivity estimated by this modeling effort suggest that riverbed internal colmation [*Brunke*, 1999] has likely impacted vertical exchange rates and hyporheic flow paths. Literature values for clay and silt loam range 0.18–0.26 W m^{-1} $°C^{-1}$ and for soil organic matter an average of 0.25 W m^{-1} $°C^{-1}$ [*Stonestrom and Blasch*, 2003]. *Bianchin et al.* [2010] found thermal conductivity through calibration of organic deposits to be 0.15 W m^{-1} $°C^{-1}$. *McKenzie et al.* [2007] reported a range though modeling wetlands of 0.1–0.5 W m^{-2} $°C^{-1}$. Analyses presented herein indicate the optimal value for the shallow zone is less than 0.5 W m^{-1} $°C^{-1}$ and the deep zone to be range much higher 0.86–2.58 W m^{-1} $°C^{-1}$. Subsequent examination of the solution space for each shallow observation indicate a lower range of values would have been needed (0.1–0.5 W m^{-2} $°C^{-1}$) to uniquely identify the optimal value. Recent work by *Descloux et al.* [2010] found hydraulic conductivity to be the most accurate method for determining riverbed colmation. On the basis of the results presented herein, it is conceivable that thermal conductivity estimated through heat flow modeling can be included in studies to identify areas impacted by colmation or deposition of fine-grained organic matter into the riverbed.

[48] There were order of magnitude differences between the estimated shallow, deep, and low-permeability zone K_z values. As shown in Table 4, the optimal values for vertical hydraulic conductivity for the shallow, low-permeability, and deep zones was predicted to be 0.22, 0.0019, and 0.018 m h^{-1}, respectively. These results along with the interpretation of the measured streambed temperature envelopes, VHGs, and pressure data support our three zone conceptual model. The low-permeability zone between the upper and lower zones was required in the model to correctly simulate the large negative VHGs measured beneath the riffle section, and the lack of vertical heat transport measured in this section of the study area.

6. Conclusions

[49] This study demonstrates the use of continuous temperature and pressure data to calibrate a longitudinal two-dimensional hyporheic exchange model during variable discharge conditions within a riffle-pool sequence. Model calibration was improved when temperature was included with pressure in determining optimal hydraulic conductivity values. We used a single and multiobjective calibration approach to estimate hydraulic conductivity in the vertical and horizontal directions and to estimate 2-D seepage rates beneath the river. The development of a 2-D longitudinal model improved our understanding of the geological controls on hyporheic flow paths. The calibrated flow model will be used for simulating arrival times and nutrient transport in the Truckee River hyporheic flow system. This is the first application of combining temperature and pressure to determine the hydraulic and thermal properties and evaluate the predictive uncertainty of simulated fluxes within a 2-D longitudinal hyporheic flow system.

[50] Hyporheic flow is multidimensional, and is controlled by riverbed topography, stage, and subsurface heterogeneity. The longitudinal 2-D flow model developed for this study area indicates the magnitude of fluid flux is greater in the horizontal than the vertical direction in all locations (Table 3). Using heat as a tracer in longitudinal exchange approach presents a unique challenge for estimating horizontal hydraulic conductivity because of the relatively short and multidirectional flow paths with a mixture of upwelling and downwelling directions. In deeper deposits, the hydraulic conductivity at each location can be identified reliably by this approach and could be extended to 3-D simulations. Although analytical methods have strengths in estimating flux in the vertical direction, analytical approaches would not have been appropriate in the present study. Furthermore, simply estimating the seepage rate through the riverbed interface would not have provided information regarding the hyporheic flow paths, and ultimately, the fate and transport of nutrients in the study area.

[51] The methods presented in this paper outline a calibration approach for estimating hydraulic and thermal properties beneath a river that are not easily measureable by traditional methods. Characterizing heterogeneity and the effects on flow direction and magnitude is crucial in understanding nutrient transport in the hyporheic zone. This approach has great potential toward characterizing hydraulic and thermal properties in heat as a tracer applications where multidirectional fluid flow is to be determined.

[52] **Acknowledgments.** Support for the first author was provided by the U.S. EPA Landscape Ecology Branch, Las Vegas. Support for the second author was provided by the U.S. Geological Survey's Groundwater Resources Program through the Office of Groundwater. We wish to thank the Pyramid Lake Paiute Tribe for permitting access to and instrumentation of the Truckee River on their property. We also want to thank Greg Pohll, Dave Prudic for insightful discussions, and Seshadri Rajagopal for helpful MATLAB programming assistance. Earlier versions of this manuscript

benefited from comments by Michael N. Gooseff and Kenneth E. Bencala. Comments by Ty Ferre and an anonymous reviewer also led to significant improvements to the manuscript.

References

Anderson, M. P. (2005), Heat as a ground-water tracer, *Ground Water*, *43*, 951–968.

Bartolino, J. R., and R. G. Niswonger (1999), Numerical simulation of vertical ground-water flux of the Rio Grande from ground-water temperature profiles, central New Mexico, *U.S. Geol. Surv. Water Resour. Invest. Rep., 99-4212*, 1–34, USGS, Albuquerque, NM.

Bencala, K. E. (2011), Stream-Groundwater Interactions, *Treatise on Water Science*, vol. 2, edited by P. Wilderer, pp. 537–546, Academic, Oxford, U. K., doi:10.1016/B978-0-444-53199-5.00115-9.

Beven, K. J. (2006), A manifesto for the equifinality thesis, *J. Hydrol.*, *320*, 18–36.

Beven, K. J., and J. Freer (2001), Equifinality, data assimilation and uncertainty estimation in mechanistic modelling of complex environmental systems using the GLUE methodology, *J. Hydrol.*, *249*(1–4), 11–29.

Bianchin, M., L. Smith, and R. Beckie (2010), Quantifying hyporheic exchange in a tidal river using temperature time series, *Water Resour. Res.*, *46*, W07507, doi:10.1029/2009WR008365.

Boulton, A. (2007), Hyporheic rehabilitation in rivers: Restoring vertical connectivity, *Freshwater Biol.*, *52*, 632–650.

Boulton, A. J., T. Datry, T. Kasahara, M. Mutz, and J. A. Stanford (2010), Ecology and Management of the hyporheic zone: River-groundwater interactions of running waters and their floodplains, *J. North Am. Benthol. Soc.*, *29*(1), 26–40.

Bower, H., and R. C. Rice (1976), A slug test for determining hydraulic conductivity of unconfined aquifers with completely or partially penetrating wells, *Water Resour. Res.*, *12*(3), 423–428.

Bowker-Davy, J., W. Sweeting, N. Wright, R. T. Clark, and S. Arnott (2006), The distribution of benthic and hyporheic macroinvertebrates from the heads and tails of riffles, *Hydrobiologia*, *563*, 109–123.

Bravo, H. R., F. Jiang, and R. J. Hunt (2002), Using groundwater temperature data to constrain parameter estimation in a groundwater flow model of a wetland system, *Water Resour. Res.*, *38*(8), 1153, doi:10.1029/2000WR000172.

Brunke, M. (1999), Colmation and depth filtration within riverbeds: Retention of particles in hyporheic interstices, *Int. Rev. Hydrobiol.*, *84*, 99–117.

Brunke, M., and T. Gonser (1997), The ecological significance of exchange processes between rivers and groundwater, *Freshwater Biol.*, *37*, 1–33.

Cardenas, M. B., J. L. Wilson, and V. A. Zlotnik (2004), Impact of heterogeneity, bed forms and river curvature on subchannel hyporheic exchange, *Water Resour. Res.*, *40*, W08307, doi:10.1029/2004WR003008.

Conant, B. (2004), Delineating and quantifying ground water discharge zones using riverbed temperatures, *Ground Water*, *42*, 243–257.

Constantz, J. (2008), Heat as a tracer to determine riverbed water exchanges, *Water Resour. Res.*, *44*, W00D10, doi:10.1029/2008WR006996.

Dahm, C. N., C. Baxter, H. M. Valett, and W. Woessner (2006), Hyporheic zones, in *Methods in Stream Ecology*, edited by F. R. Hauer and G. A. Lamberti, pp. 119–142, Academic, Boston, Mass.

Dahm, C. N., N. B. Grimm, P. Marmonier, H. Valett, and P. Vervier (1998), Nutrient dynamics at the interface between surface water and groundwater, *Freshwater Biol.*, *40*, 427–451.

Day-Lewis, F. D., E. A. White, C. D. Johnson, and J. W. Lane Jr. (2006), Continuous resistivity profiling to delineate submarine groundwater discharge: Examples and limitations, *Leading Edge*, *25*, 724–728.

Descloux, S., T. Datry, M. Phillippe, and P. Marmonier (2010), Comparison of different techniques to assess surface and subsurface streambed colmation with fine sediments, *Int. Rev. Hydrobiol.*, *95*, 520–540, doi:10.1002/iroh.201011250.

Doherty, J. (2003), Ground water model calibration using pilot points and regularization, *Ground Water*, *41*, 170–177.

Doussan, C., A. Toma, B. Paris, G. Poitevin, E. Ledoux, and M. Detay (1994), Coupled use of thermal and hydraulic head data to characterize river-groundwater exchanges, *J. Hydrol.*, *153*, 215–229.

Duan, Q., V. K. Gupta, and S. Sorroshian (1992), Effective and efficient global optimization for conceptual rainfall-runoff models, *Water Resour. Res.*, *28*(4), 1015–1031.

Ferguson, G., and V. Bense (2011), Uncertainty in 1D heat-flow analysis to estimate groundwater discharge to a river, *Ground Water*, *49*, 336–347.

Findlay, S. (1995), Importance of surface-subsurface exchange in river ecosystems: The hyporheic zone, *Limnol. Oceanogr.*, *40*, 159–164.

Franken, R. J. M., R. G. Storey, and D. D. Williams (2001), Biological, chemical, and physical characteristics of downwelling and upwelling zones in the hyporheic zone of a north-temperate river, *Hydrobiologia*, *444*,183–195.

Freer, J., K. Beven, and B. Ambroise (1996), Bayesian estimation of uncertainty in runoff prediction and the value of data: An application of the GLUE approach, *Water Resour. Res.*, *32*(7), 2161–2173.

Gooseff, M. N., J. K. Anderson, S. M. Wondzell, J. LaNier, and R. Haggerty (2006), A modeling study of hyporheic exchange pattern and the sequence, size, and spacing of river bedforms in mountain river networks, Oregon, USA, *Hydrol. Processes*, *20*(11), 2443–2457.

Halford, K. J., and E. L. Kuniansky (2002), Documentation of spreadsheets for the analysis of aquifer-test and slug-test data, *U.S. Geol. Surv. Open File Rep., 02-197*.

Harvey, J. H., and K. E. Bencala (1993), The effect of riverbed topography on surface-subsurface water exchange in mountain catchments, *Water. Resour. Res.*, *29*(1), 89–98, USGS, Carson City, NV.

Hatch, C. E., A. T. Fisher, J. S. Revenaugh, J. Constantz, and C. Ruehl (2006), Quantifying surface water–groundwater interactions using time series analysis of riverbed thermal records: Method development, *Water Resour. Res.*, *42*, W10410, doi:10.1029/2005WR004787.

Healy, R. W. (1990), Simulation of solute transport in variably saturated porous media with supplemental information on modifications to the U.S. Geological Survey's computer program VS2D, *U.S. Geol. Surv. Water Resour. Invest. Rep., 90-4025*, USGS, Denver, CO.

Healy, R. W., and A. D. Ronan (1996), Documentation of computer program VS2DH for simulation of energy transport in variably saturated porous media: Modification of the U.S. Geological Survey's computer program VS2DT, *U.S. Geol. Surv. Water Resour. Invest. Rep., 96-4230*, 36 pp., USGS, Denver, CO.

Hornberger, G. M., and R. C. Spear (1981), An approach to the preliminary analysis of environmental systems, *J. Environ. Manage.*, *12*, 7–18.

Hsieh, P. A., W. Wingel, and R. W. Healy (2000), VS2DHI—A graphical software package for simulating fluid flow and solute of energy transport in variably saturated porous media, *U.S. Geol. Surv. Water Resour. Invest. Rep., 99-4230*, 16 pp., Denver, CO.

Kalbus, E., F. Reinstorf, and M. Schirmer (2006), Measuring methods for groundwater-surface water interactions: A review, *Hydrol. Earth Syst. Sci.*, *10*, 873–887.

Kasahara, T., and S. M. Wondzell (2003), Geomorphic controls on hyporheic exchange flow in mountain streams, *Water Resour. Res.*, *39*(1), 1005, doi:10.1029/2002WR001386.

Käser, D. H., A. Binley, L. A. Heathwaite, and S. Krause (2009), Spatio-temporal variations of hyporheic flow in a riffle-step pool sequence, *Hydrol. Processes*, *23*, 2138–2149, doi:10.1002/hyp.7317.

Keery, J., A. Binley, N. Crook, and J. W. N. Smith (2007), Temporal and spatial variability of groundwater-surface water fluxes: Development and application of an analytical method using temperature time series, *J. Hydrol.*, *336*(102), 1–16.

Lapham, W. W. (1989), Use of temperature profiles beneath streams to determine rates of vertical ground-water flow and vertical hydraulic conductivity, *U.S. Geological Survey Water Supply Paper*, 2337, 1–35. Denver, CO.

Lautz, L. K. (2010), Impacts of nonideal field conditions on vertical water velocity estimates from streambed temperature time series, *Water Resour. Res.*, *46*, W01509, doi:10.1029/2009WR007917.

Lautz, L. K., N. T. Kranes, and D. I. Siegel (2010), Heat tracing of heterogeneous hyporheic exchange adjacent to in-stream geomorphic features, *Hydrol. Processes*, *24*, 3074–3086.

Loheide, S. P., and S. M. Gorelick (2006), Quantifying river-aquifer interactions through the analysis of remote sensed themographic profiles and in-situ temperature histories, *Environ. Sci. Technol.*, *40*, 336–3341.

McKenzie, J. M., D. I. Siegel, D. O. Rosenberry, P. H. Glaser, and C. I. Voss (2007), Heat transport in the Red Lake Bog, Glacial Lake Agassiz Peatlands, *Hydrol. Processes*, *21*, 369–378. doi:10.1002/hyp.

Mermillod-Blondin, F., M. Creuze des Chatelliers, P. Marmonier, and M. J. Dole-Olivier (2000), Distribution of solutes, microbes and invertebrates in river sediments in river sediments along a riffle-pool-riffle sequence, *Freshwater Biol.*, *44*, 255–269.

Neilson, B. T., D. K. Stevens, S. C. Chapra, and C. Bandaragoda (2011), Two-zone transient storage modeling using temperature and solute data with multiobjective calibration: 2. Temperature and solute, *Water Resour. Res.*, *46*, W12521, doi:10.1029/2009WR008759.

Niswonger, R. G., and G. E. Fogg (2008), Influence of perched groundwater on base flow, *Water Resour. Res.*, *44*, W03405, doi:10.1029/2007WR006160.

Niswonger, R., and D. E. Prudic (2003), Modeling heat as a tracer to estimate riverbed seepage and hydraulic conductivity, in *Heat as a Tool for Studying the Movement of Ground Water Near Rivers*, edited by J. Constantz and D. A. Stonestrom, vol. 1260, 73–78, U.S. Geol. Surv. Circ., USGS, Denver, CO.

Niswonger, R., and J. L. Rupp (2000), Monte Carlo analysis of riverbed seepage rates, in *Riparian Ecology and Management in Multi-land Use Watersheds*, edited by P. J. Wigington and R. C. Beschta, pp. 161–166, Am. Water Resour. Assoc., Middleburg, Va.

Niswonger, R. G., D. E. Prudic, G. Pohll, and J. Constantz (2005), Incorporating seepage losses into the unsteady river flow equations for simulating intermittent flow along mountain front rivers, *Water Resour. Res.*, *41*, W06006, doi:10.1029/2004WR003677.

Packman, A. I., and J. S. MacKay (2003), Interplay of river-subsurface exchange, clay particle deposition and riverbed evolution, *Water Resour. Res.*, *39*(4), 1097, doi:10.1029/2002WR001432.

Ronan, A. D., D. E. Prudic, and C. E. Thodal, and J. Constantz (1998), Field study and simulation of diurnal temperature effects on infiltration and variably saturated flow beneath an ephemeral river, *Water Resour. Res.*, *34*, 2137–2153, doi:10.1029/98WR01572.

Selker, J., N. van de Giesen, M. Westholf, W. Luxemburg, and M. B. Parlange (2006), Distributed fiber-optic temperature sensing for hydrologic systems, *Water Resour. Res.*, *42*, W12202, doi:10.1029/2006WR005326.

Shanafield, M., C. Hatch, and G. Pohll (2011), Uncertainty in thermal time series analysis estimate of streambed water flux, *Water Resour. Res.*, *47*, W03504, doi:10.1029/2010WR009574.

Song, J., X. Chen, C. Cheng, S. Summerside, and F. Wen (2007), Effects of hyporheic processes on riverbed vertical hydraulic conductivity in three rivers of Nebraska, *Geophys. Res. Lett.*, *34*, L07409, doi:10.1029/2007GL029254.

Stallman, R. W. (1963), Methods of collecting and interpreting ground-water data, paper presented at U.S. Geol. Surv. Water Supply Pap., 1544-H, 36–46, Reston, VA.

Stallman, R. W. (1965), Steady one-dimensional fluid flow in a semiinfinite porous medium with sinusoidal surface temperature, *J. Geophys. Res.*, *70*, 2821–2827, doi:10.1029/JZ070i012p02821.

Stonestrom, D. A., and K. W. Blasch (2003), Determining temperature and thermal properties for heat-based studies of surface-water ground-water interactions, in *Heat as a Tool for Studying the Movement of Ground Water Near Rivers*, edited by J. Constantz and D. A. Stonestrom, vol. 1260, 73–78, U.S. Geol. Surv. Circ., Denver, CO.

Stonestrom, D., and J. Constantz (2003), Heat as a tracer of water movement near rivers, *U.S Geol. Survey Circ.*, *1260*, 1–96.

Storey, R. G., K. W. F. Howard, and D. D. Williams (2003), Factors controlling riffle-scale hyporheic exchange flows and their seasonal changes in a gaining river: A three-dimensional groundwater flow model, *Water Resour. Res.*, *39*(2), 1034, doi:10.1029/2002WR001367.

Suzuki, S. (1960), Percolation measurements based on heat flow through soil with special reference to paddy fields, *J. Geophys. Res.*, *65*, 2883–2885, doi:10.1029/JZ065i009p02883.

Triska, F. J., J. H. Duff, and R. J. Avanzino (1993), The role of water exchange between river channel and its hyporheic zone on nitrogen cycling at the terrestrial-aquatic interface, *Hydrobiologia*, *251*, 167–184.

Valett, H. M., S. G. Fisher, N. B. Grimm, and P. Camill (1994), Vertical hydrologic exchange and ecological stability of a desert river ecosystem, *Ecology*, *75*, 548–560.

Vaux, W. G. (1968), Intragravel flow and interchange of water in a riverbed, *Fish. Bull.*, *66*, 479–489.

Vrugt, J. A., H. V. Gupta, W. Bouten, and S. Sorooshian (2003), A shuffled complex evolution Metropolis algorithm for optimization and uncertainty assessment of hydrologic model parameters, *Water Resour. Res.*, *39*(8), 1201, doi:10.1029/2002WR001642.

Wagener, T., and J. Kollat (2007), Numerical and visual evaluation of hydrological and environmental models using the Monte Carlo analysis toolbox, *Environ. Modell. Software*, *22*, 1021–1033.

Wagener, T., D. P. Boyle, M. J. Lees, H. S. Wheeter, H. V. Gupta, and S. Sorooshian (2001), A framework for development and application of hydrologic models, *Hydrol. Earth Syst. Sci.*, *5*(1), 13–26.

Winter, T. C., J. W. Harvey, O. L. Franke, and W. M. Alley (1998), Ground water and surface water: A single resource, *U.S. Geol. Surv. Circ.*, *1139*.

White, D. S. (1993), Perspectives on defining and delineating hyporheic zones, *J. North Am. Benthol. Soc.*, *12*, 61–69.

Woessner, W. W. (2000), River and fluvial plain ground water interactions: Rescaling hydrogeologic thought, *Ground Water*, *38*, 423–429.

Young, P. C. (1978), A general theory of modeling for badly defined dynamic systems, in *Modeling, Identification and Control in Environmental Systems*, edited by G. C. Vansteenkiste, pp. 103–135, North Holland, Amsterdam.

C. Davis, Division of Earth and Ecosystem Sciences, Desert Research Institute, 2215 Raggio Pkwy., Reno, NV 89512, USA.

A. Mckay and R. C. Naranjo, Division of Hydrologic Sciences, Desert Research Institute, 2215 Raggio Pkwy., Reno, NV 89512, USA. (naranjo@dri.edu)

R. G. Niswonger, U. S. Geological Survey, 2730 N. Deer Run Rd., Carson City, NV 89701, USA.

M. Stone, Department of Civil Engineering, University of New Mexico, MSC01-1070, Albuquerque, NM 87131, USA.